ELSEVIER

Tectonophysics 356 (2002) 323–336

TECTONOPHYSICS

www.elsevier.com/locate/tecto

Analogue models of orogenic wedges controlled by erosion

Katarina S. Persson [a,*], Dimitrios Sokoutis [b]

[a] *Hans Ramberg Tectonic Laboratory, Geodynamics and Tectonics, Uppsala University, Villavägen 16, SE-752 36 Uppsala, Sweden*
[b] *The Netherlands Center for Integrated Solid Earth Science, Faculty of Earth and Life Sciences, Vrije Universiteit, De Boelelaan 1085, 1081 HV Amsterdam, Netherlands*

Received 21 November 2001; accepted 9 August 2002

Abstract

Indentation in the upper brittle crust where one plate is stiffer than the other produces vertical extrusion of a doubly vergent orogenic wedge. Sandbox models of this process show that erosion with or without deposition of the eroded material onto one or both margins significantly changes the internal patterns of orogenic shear and compaction within the orogens. Erosion decreases the vertical stress and changes the criticality of the orogenic wedge, whereas redeposition increases the vertical stress on its margins.

Effective indenters of accreted sand, which develop in models without erosion if the rigid indenter face dip is 75° (e.g., >45°) or ≤ 15 are strongly affected by erosion. Rapid erosion favors thrusting over compaction and decreases both the size and the relevance of the effective indenters. Redeposition of eroded material on the margins also expands the lifetime of the active shear as the additional load delays initiation of underlying new shears.

Keywords: Erosion; Orogenic wedges; Sandbox modelling; Deposition; Indenter

1. Introduction

One of the most impressive characteristics of orogeny is the vertical escape of wedges of deep metamorphic rocks extruded between thrust ramps during the continental convergence that follows continental suturing. Where one converging continent is stronger than the other (e.g., Tapponnier and Molnar, 1976), ratios of vertical to lateral escape during indentation depend on the degree of orogen-lateral confinement of the indented continent (e.g., Davy and Cobbold, 1988). The nature of escape also depends on layer rheologies, the dimensions of indented and indenting continents, and the rate of erosion and sedimentation affecting the area (Davy and Cobbold, 1988, 1991; Beaumont et al., 1992; Cobbold et al., 1993). Whereas strong orogen-lateral confinement of the indented plate leads to crustal thickening, weak lateral confinement favors lateral escape (Tapponnier et al., 1982; Davy and Cobbold, 1988; Ratschbacher et al., 1991).

The exhumation of high-grade metamorphic rocks during continental convergence is mainly due to tectonic denudation and/or erosion (Beaumont et al., 1992; Koons, 1990; Thompson et al., 1997) and related isostatic adjustment (Merle, 1994). Denudation

* Corresponding author.
E-mail address: Katarina.Persson@geo.uu.se (K.S. Persson).

0040-1951/02/$ - see front matter © 2002 Elsevier Science B.V. All rights reserved.
PII: S0040-1951(02)00443-2

by gravity-induced collapse unroofs compressional orogens and exhumes material from within the orogen in proportion to the mass removed. Unroofing disturbs the criticality of the deforming wedge by reducing the component of the stress tensor within the wedge due to the weight of overburden (Beaumont et al., 1992). As overburden is removed, the yield strength of the Coulomb (frictional) upper crust decreases so that additional deformation follows. Erosion, on the other hand, has often been considered a passive process, not one that can control tectonic evolution. However, several orogens that suffer severe erosion are characterized by a high exhumation rate (Koons, 1990). Furthermore, sedimentation of the eroded material can increase the vertical principal stresses on one or both margins of the wedge. The rate of erosion is dependent on factors such as climate, rock-type, topography and rate of convergence.

This paper focuses on strain partitioning during continental convergence, as affected by erosion and sedimentation. Sandbox models, where strong orogen-lateral confinements enforce crustal thickening by vertical escape during indentation, have been subjected to erosion and sedimentation at three different rates. Observations from these sandbox models suggest the dominant deformation mechanisms (compaction, slip along the basal décollement or formation of thrust planes) as well as the expected thrust geometries in profile. Understanding the effect of erosion and sedimentation of the deep levels of orogenic wedges will ease interpretations of geophysical profiles.

2. Previous modelling and terminology

The bulldozer model (Davis et al., 1983), where a blade accretes a prism of frictional material in one direction, has been useful for discussing the concept of criticality and the asymmetric accretion of sediments above subduction zones with vertical indenters of infinite height (Dahlen, 1988; Mulugeta, 1988; Mulugeta and Koyi, 1987, 1992; Huiqi et al., 1992; Marshak and Wilkerson, 1992). However, it is insufficient for describing continental convergence zones, where the indenting and indented plates are of approximately the same vertical dimensions so that the rising wedge can spread equally over the indenting and indented continents (Fig. 1), creating a double vergent orogenic wedge (Malavieille, 1984; Koons, 1990; Beaumont et al., 1992; Storti et al., 2000). This "pop-up" wedge, bound by fore- and back-kinks with dips α and β (Fig. 1), is typical for materials with an internal friction angle of 30° (Colletta et al., 1991). To illustrate orogenic wedges, this work used rigid indenters driven into sand packs of the same thickness and same passive strata. The orogenic wedge is represented in the model as the area between the fore-kink and back-kink active at any one time (Fig. 1). The principal stresses within the rising model orogenic wedge are defined by local relations between the angle of internal friction of the sand, the angle of friction of the décollement, the topographic slope, and the dip of the décollement (Koons, 1990).

Strain in sand packs localizes on small-scale fault-like structures (Mandle, 1988; Willett et al., 1993),

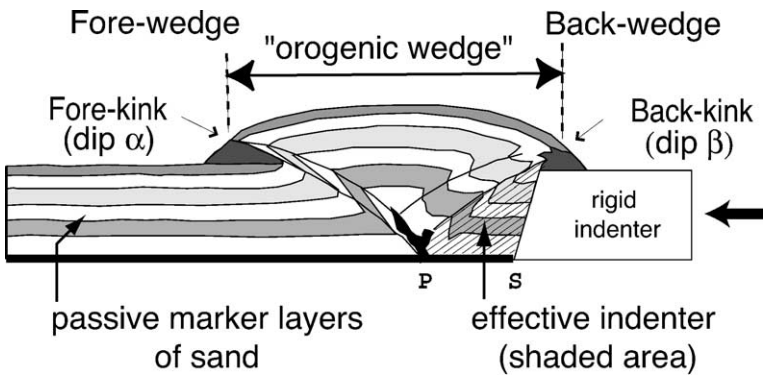

Fig. 1. Sandbox model of orogenic wedge bound by fore- and back-kinks, where the back-kink is the front face of an effective indenter. The back- and fore-kinks develop and propagate from a point, P, along the base of the model. Arrow indicates movement direction of the rigid indenter. The dips α and β are the angles between the base of the model and the fore-kink and back-kink, respectively.

here called "*kinkbands or kinks*". According to Coulomb theory, initial failure occurs by dilation along zones with initial angles of $\pm[45-(\Phi/2)]$ to the principal axes of stress, where Φ is the coefficient of internal friction (Willett et al., 1993). Kinkbands start to dilate and shear at a finite width, but progressively narrow to *shear* zones and then to *thrust* zones that define the bottom boundary of each successive imbricate slice. The deformation mechanisms within the sand packs are lateral compaction, basal slip and imbricate shearing or kinking (Mulugeta, 1988; Mulugeta and Koyi, 1987, 1992). Although indentation is steady, deformation of the sand pack is episodic. The wedge rises stepwise and each of these incremental rises predates the formation of a new kink (Mulugeta and Koyi, 1992; Koyi, 1995).

The definition of fore-kink and back-kink in this work is based on the movement direction of the rigid indenter. Structures that propagate forward, away from the advancing indenter with progressive shortening, are called *fore-kinks*; those that propagate backward, towards the indenter, are called *back-kinks* (Fig. 1).

Recent sandbox models of crustal wedges that escape vertically demonstrate a strong control by the vertical shape of the rigid indenter (Bonini et al., 1999; Persson, 2001). In models where the dip of the rigid indenter face differs from the angle of internal friction of sand ($\sim 30^\circ$), sand is transferred to the front of the rigid indenter so that the system builds its own effective indenter by accreting and compacting sand between the rigid indenter and an active back-shear. This back-shear was taken to be the front face of the "effective indenter" (Fig. 1) (Bonini et al., 1999), and its dip is controlled by the angle of internal friction of the sand. The back-shear propa-

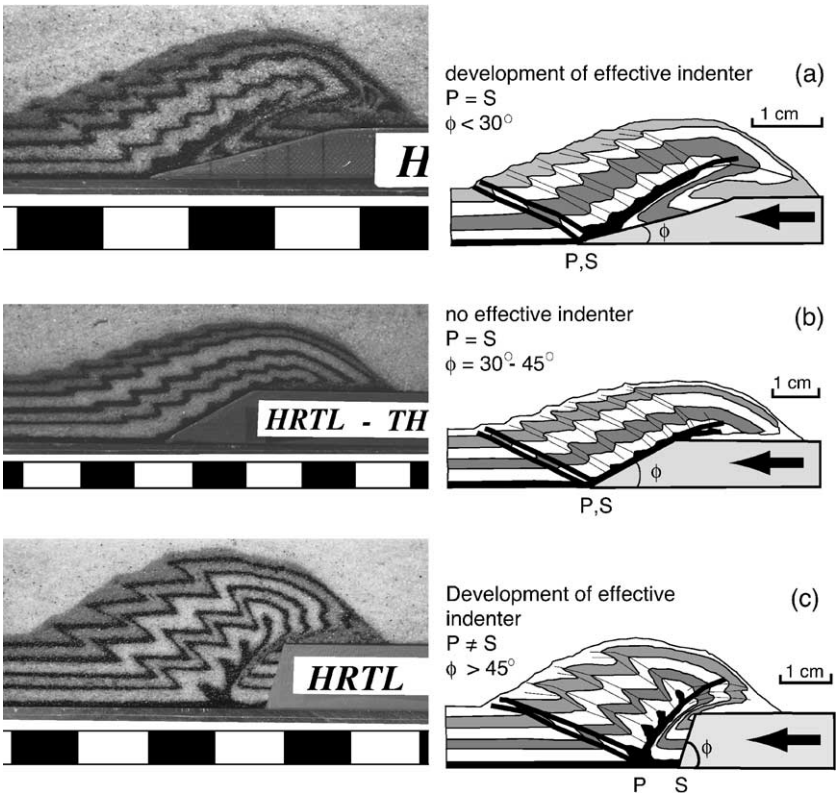

Fig. 2. Models divided into three groups (a), (b) and (c), after Bonini et al. (1999) and Persson (2001). P is the point from where the back-shear propagates. S is the toe of the rigid indenter (cf. the velocity discontinuity in numerical model by Beaumont et al., 1992).

gates simultaneously with a fore-kink from a line along the base of the sand pack. The line, representing the toe of the effective indenter, intercepts vertical longitudinal profiles at a "P"- or Propagation point (Fig. 1) (Bonini et al., 1999). With progressing convergence, successive back-kinks and fore-kinks propagate alternatively from the P-point. Bonini et al., (1999) divided their analogue models into two groups. The first group consisted of the models where the face of the rigid indenter dipped at $\leq 45°$. In those models, the first kinks developed at the toe of the rigid indenter and the rigid indenter face was used as the active shear plane for the back-shear. The second group consisted of models with rigid indenters with face dips of $\geq 60°$. These models developed an effective indenter between the first back-kink, and the face of the rigid indenter where the back-kink propagated from a P-point in front of the toe of the rigid indenter (i.e., >45°, Persson, 2001) (Fig. 2b and c). Persson (2001) added another situation where effective indenters develop; namely, in front of low-angle rigid indenters with face dips of 15°. However, in those models, the P-point coincided with the toe of the rigid indenter (Fig. 2a).

Merle and Abidi (1995) used sandbox modelling to show that erosion of the relief of the developing wedge is more important than friction in keeping a shear plane active. Friction that resists movement along the shear plane is reduced by erosion. Erosion helps a particular shear plane to remain active instead of partitioning strain by developing a new shear plane. This was also shown by four-layer models of the continental lithosphere, where both erosion and sedimentation were taken into account (Cobbold et al., 1993). Merle and Abidi (1995) used a rigid indenter with a face dip of 30°, which was sufficiently close to the internal friction of the sand for no effective indenter to develop. In their experiment, the sand pack was driven towards the indenter, whereas in this study, the indenter was driven into the sand pack. The set of experiments described here used rigid indenters with front face dips of 15°, 30° and 75° to study the influence of erosion on the development of effective indenters. Merle and Abidi (1995) removed all the eroded material, but in this study, the sand was redepositioned locally.

3. Experimental material, design and procedure

Dry quartz sand of ≤ 0.25 mm in diameter, a Mohr–Coulomb material with density of 1.300 kg/m^3 and an angle of internal friction of about 30°, was used to represent the brittle behavior of the upper continental crust (Byerlee, 1978). A density of 2.700 kg/m^3 for natural rock gives a density ratio (ρ^*) between nature/model of about 0.5. A brittle upper crust, 15 km thick, is represented by 1 cm sand in the model, giving a length ratio, $L^* \sim 6 \times 10^{-7}$. As the model is performed in a normal gravity field, the nature/model gravity ratio (g^*) is 1. The vertical stress ratio (σ^*) $= \rho^* g^* L^*$ (Weijermars and Schmeling, 1986) is here then $\sim 3 \times 10^{-7}$. The cohesion T_0 of rocks has the dimension of stress; thus, $\tau^* = \sigma^*$. The measured cohesion of 90 Pa of the sand then implies a value of $\sim$ 300 MPa (T_0) for natural rocks, a value within the range listed by Goodman (1988).

Models with horizontal dimensions of 9.5 × 7 cm and vertical thickness of 1.0 cm were built in a box of rigid perspex plates (Plexiglas) (Fig. 3). Sand layers of different colors were sieved into the box to build the hanging wall. The color layers were

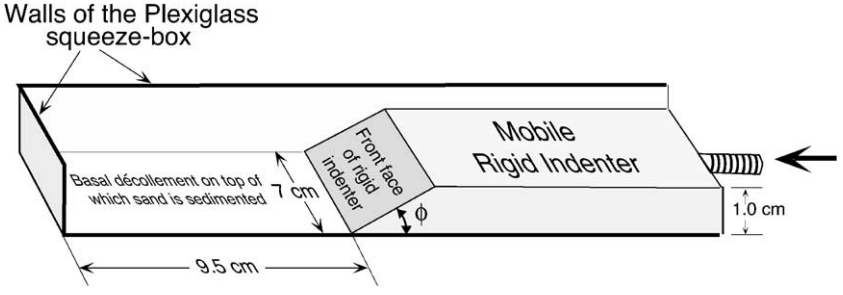

Fig. 3. Experimental design.

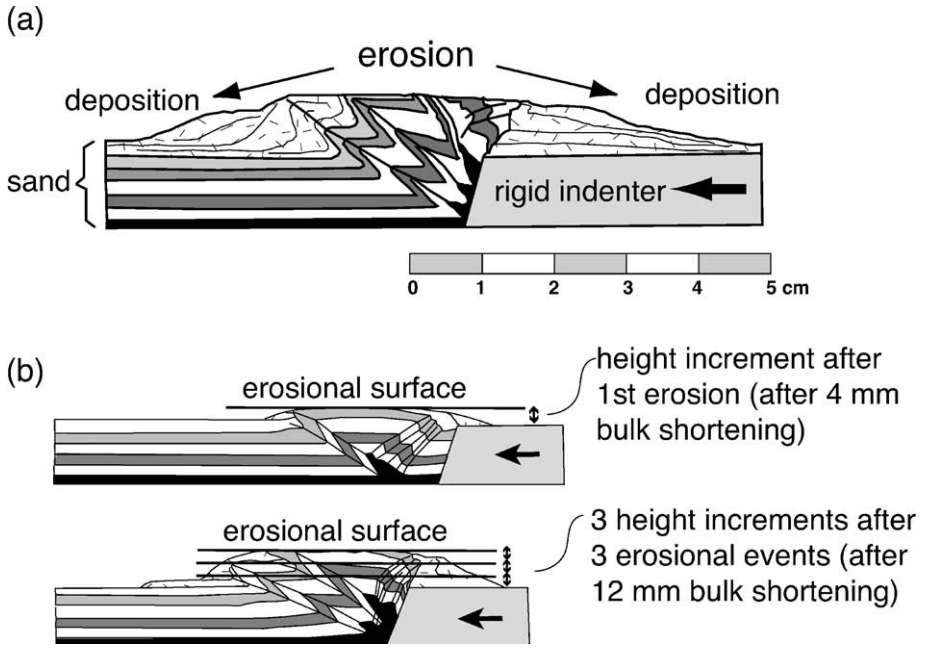

Fig. 4. Sketches illustrating (a) symmetric erosion of the extruded part of the rising wedge and deposition at the orogenic margins, and (b) measurements of height increments according to Table 1.

passive and inserted in order to visualize the internal deformation pattern.

In all models, a rigid block of plastics, representing cool crust of higher strength, was driven laterally into the sand pack at a constant displacement rate of 1.8 cm h^{-1}. However, the rate of displacement needs not be scaled precisely as Coulomb materials have a yield envelope essentially independent of strain rate (Kusznir and Park, 1984a,b; Sonder and England, 1986). The front face of the rigid indenters dipped 15°, 30° or 75° in the experiments. A value of 0.35 for the basal friction coefficient between the sand and Plexiglas floor was measured (with a method presented by Krantz, 1991).

The models were focused on the deformation of brittle upper crust decoupled from its underlying lower crust, not represented in the model, along a detachment surface represented by the Plexiglas floor of the squeezebox. All models were deformed up to 40% bulk lateral shortening.

After every 4-mm increment of lateral shortening, the top portion of the extruding wedge was spread symmetrically with a scraper both forward and backward to simulate erosion of the orogenic wedge and prograding sedimentation towards both sides

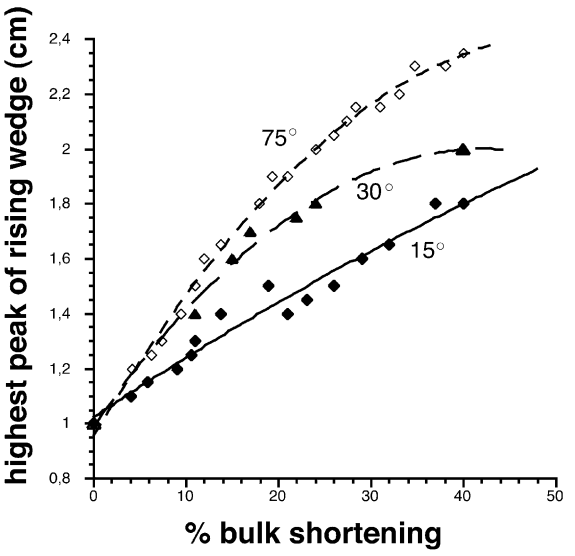

Fig. 5. Height of rising wedge with progressive Bulk lateral Shortening (B.S.) for models, where rigid indenter face dips at 15°, 30° and 75°, and there is no erosion.

(Fig. 4). If the wedge was not sufficiently high after one 4-mm increment of shortening, the next phase of erosion took place after an additional 4 mm of shortening. Three erosion rates were applied: (a) limited erosion, (b) moderate erosion, and (c) total erosion. The rate of vertical rise of the sand wedge during compression depends on the rigid indenter geometry (Persson, 2001). Wedges in models where the indenter face dips at 75° rise faster than models where the face dips at 30° and 15° (Fig. 5). Different height increments were therefore applied in relation to the rigid indenter dip. Limited erosion was where the vertical rise of the sand wedge was allowed to grow with increments of 1.5 mm when the rigid indenter dip was 75°, 1.0 mm when the rigid indenter face dip was 30°, and 0.75 mm for indenter face dips of 15°, before each phase of erosion (Table 1). For moderate erosion, the height increments were 1.0 mm for rigid indenter face dips of 75°, 0.75 mm for 30° and 0.5 mm for dips of 15° (Table 1). Total erosion kept the sand wedge at the initial level of 1.0 cm throughout the whole deformation for all models, and the eroded material was removed (Table 1). Additional models were made with asymmetric erosion for comparison. In these models, the scraping was concentrated only to the back-wedge of the model using the same technique as previously described (Table 1).

During deformation, the models were measured and photographed at regular intervals. After shortening, the models were cut to observe longitudinal cross-sections.

Table 1
The height increments (in mm) the models were allowed to grow during every 4-mm increment of lateral shortening

	Height increments for models with rigid indenter dips of 15° (mm)	Height increments for models with rigid indenter dips of 30° (mm)	Height increments for models with rigid indenter dips of 75° (mm)
Limited erosion	0.75	1.0	1.5
Moderate erosion	0.5	0.75	1.0
Total erosion	0	0	0

All material above those height increment was eroded and deposited equally on the hinterland and foreland (cf. Fig. 4).

4. Limitations

In nature, an increase in vertical loading, by extrusion of an orogenic wedge, results in isostatic adjustment and depression of the thrust planes on a crustal scale. In the models, this factor was not taken into account. The models focused on brittle deformation and took no account of any ductile strain within the extruded material. Temperature variations have not been considered either. The indenter was rigid and could not deform as a stronger plate might deform in nature.

In most models described here, the erosion applied to both sides of the wedge was the same although mountain ranges commonly have asymmetric rainfall patterns.

5. Results

Steady advance of the rigid indenter into all models induced horizontal forces that caused compaction of the sand and later caused slip along the décollement as the basal friction was overcome. A single back-kink and a single fore-kink developed, thus defining the wedge. When this wedge reached criticality, i.e., when the first conjugate shears seized up because of the increased weight of the wedge, a new slip occurred along the basal décollement. The area in front of the first fore-kink compacted laterally and the strain again localized to develop a new fore-kink, while the previous fore-kink became inactive and was pushed up the active back-shear.

5.1. Models with no erosion and rigid indenter face dips of 75°

In models with no erosion, rigid indenter face dips of 75° and initial thickness of 1.0 cm, kinks nucleated at a P-point in front of the rigid toe (Fig. 6a). As the deformation proceeded, the first formed fore- and back-kinks migrated upward along a single fore-thrust. During this upward transport, the lower parts of the

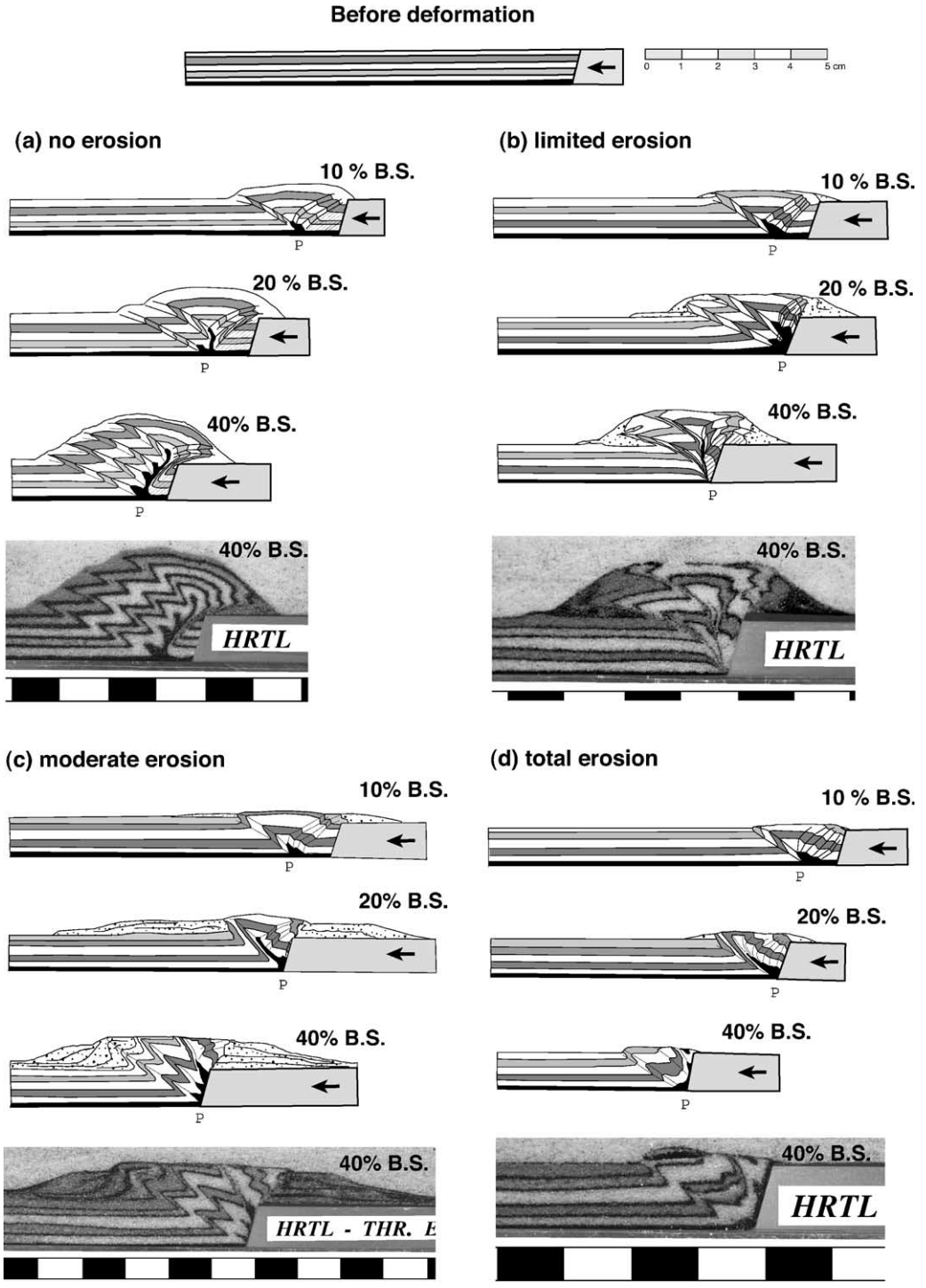

Fig. 6. Sketches of models with rigid indenter face dip of 75° after (a) no erosion; (b) limited erosion and local redeposition; (c) moderate erosion and local redeposition; and (d) total erosion, and after 10%, 20% and 40% Bulk lateral Shortening (B.S.). The effective indenter is shaded. The dotted fields represent deposited debris.

back-kink steepened due to lateral compaction near the rigid indenter. A new back-kink formed after a bulk shortening of 10% (Fig. 6a). This second back-kink deactivated, steepened and rotated as it was also carried up the fore-shear. The rising wedge was asymmetric, between a single fore-kink that nucleated with a dip of 30° (α in Fig. 1) and two back-kinks dipping at about 34° (β in Fig. 1). After 20% bulk shortening, a second fore-kink developed at a new P-point in front of the previous one (Fig. 6a). The third back-kink nucleated from this new P-point, started to form a back-shear with a dip of about 40° along which inactive fore-kinks were carried upward as new (fourth and fifth) fore-kinks developed. By 40% bulk shortening, the last-developed back-shear clearly defined the frontal part of the effective indenter, which now had a dip of about 50° (Fig. 6a). Above the edge of the rigid indenter, the back-shear flattened to a dip of 5° (Fig. 6a) similar to the back-shear in experiments of Malavieille (1984), where no rigid indenter was used.

5.2. Limited erosion and local deposition of models with rigid indenter dips of 75°

This experiment was similar to that described above, but the extruded sand was redistributed from the rising wedge symmetrically onto the sand pack and indenter.

The first fore-kink developed at a P-point in front of the rigid indenter and was clearly developed by 4% bulk shortening. This fore-kink remained active until the second formed after 17% bulk shortening (Fig. 6b). The second fore-kink also initiated in front of the rigid indenter, but stayed active until the P-point coincided with the rigid indenter. The second fore-kink developed into a fore-shear that was still active by 40% bulk shortening, whereas models without erosion had initiated a fourth fore-kink by 40% bulk shortening (cf. Fig. 6a and b). The back-shear defining the effective indenter was much steeper than in the nonerosional model (cf. Fig. 6a and b) as each kink

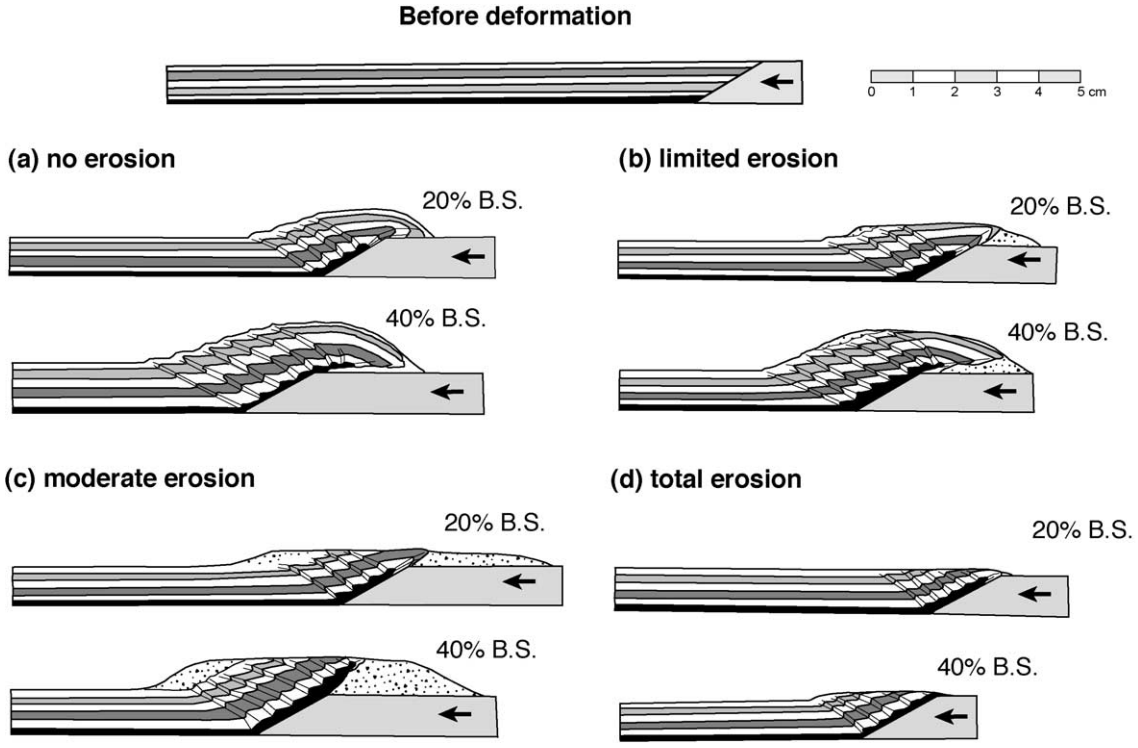

Fig. 7. Sketches of models where rigid indenter face dips at 30° after (a) no erosion; (b) limited erosion and local redeposition; (c) moderate erosion and local redeposition; and (d) total erosion, after 20% and 40% Bulk lateral Shortening (B.S.). The dotted fields represent deposited debris.

remained active for longer, steepened and back-rotated to bind an extruding fan (Fig. 6b).

5.3. Moderate erosion and sedimentation of models with rigid indenter face dips of 75°

In this model (Fig. 6c), three fore-kinks developed at 4%, 21%, and 38% bulk shortening, respectively. After the first fore-kink had developed and as the rigid indenter advanced further, the first shear plane remained active until the toe of the rigid indenter eventually caught up with the P-point. The first fore-kink was then forced up the rigid indenter as a second fore-kink developed, but by this stage, the toe of the rigid indenter and the P-point coincided (Fig. 6c). By 40% bulk shortening, the front face of the rigid indenter acted as a single back-shear, and no effective indenter could be identified. Successive new fore- and back-kinks propagated from the toe of the rigid indenter except for the very first fore- and back-kinks that had already nucleated a short distance in front of the toe of the rigid indenter before the first increment of erosion. All fore-kinks nucleated with dips of 30° and back-rotated to smaller dips. Steepening of the lower parts of the fore-kinks was less pronounced than in the models subjected to no erosion (Fig. 6a) or limited erosion (Fig. 6b). The back-kinks were severely distorted as local deposition hindered gravitational collapse of the extruded sand (Fig. 6c).

5.4. Total erosion of models with rigid indenter dips of 75°

The first fore-kink developed at less than 4% bulk shortening and remained active until ~ 21% bulk shortening, when the second fore-kink developed

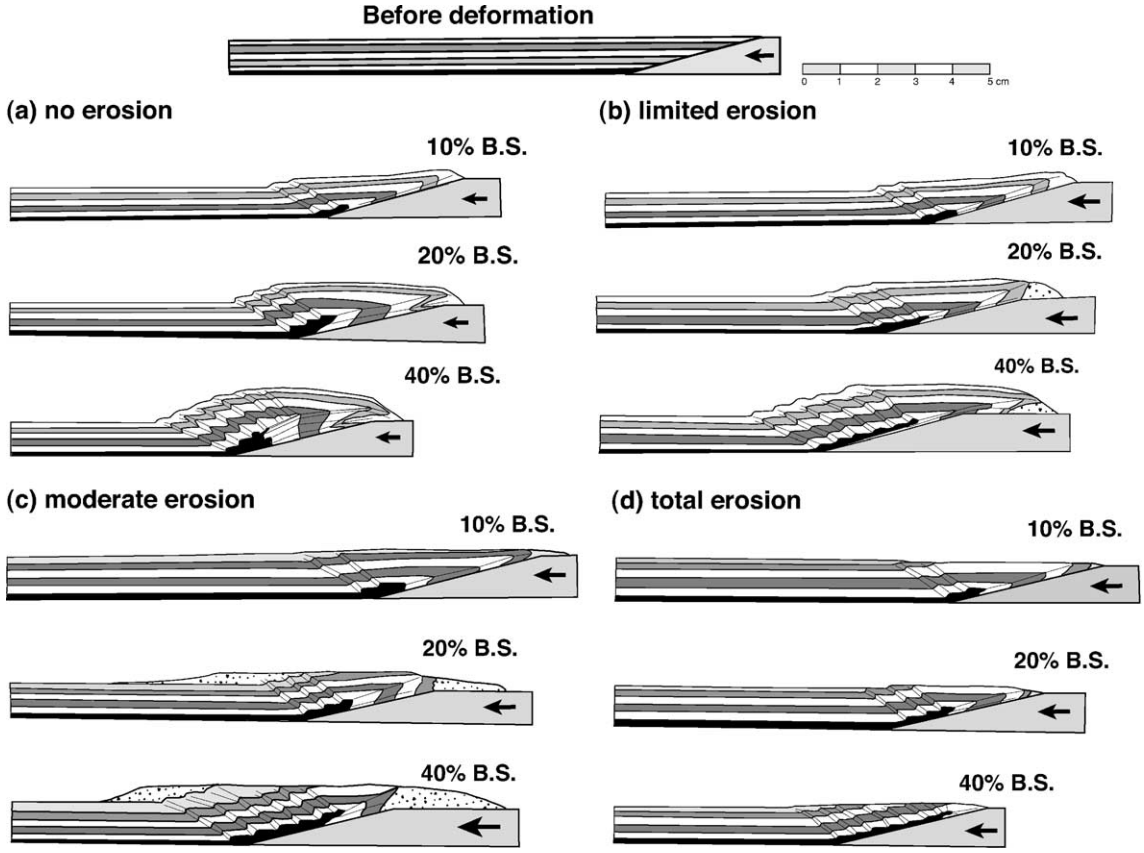

Fig. 8. Sketches of models where rigid indenter face dips at 15° after (a) no erosion; (b) limited erosion and local redeposition; (c) moderate erosion and local redeposition; and (d) total erosion, after 10%, 20% and 40% bulk lateral shortening. The dotted fields represent deposited debris.

(Fig. 6d). By 40% bulk shortening, the second fore-kink was still active (Fig. 6d). No effective indenter developed, and the front face of the rigid indenter acted as the only active back-shear throughout the experiment (Fig. 6d).

5.5. Models with rigid indenter face dips of 30°

All models developed four fore-kinks by 20% bulk shortening except models with total erosion that developed five fore-kinks (Fig. 7). By 40% bulk shortening, all models had developed seven fore-kinks (Fig. 7). However, the number of fore-kinks developed by the model with total erosion was obscured as the early fore-kinks already had been eliminated by erosion; only five fore-kinks were still visible (Fig. 7d). The fore-kinks initiated with dips of 26–32°, but steepened and rotated as a result of lateral compaction with further deformation. In models with no or limited local deposition on the hinterland above the rigid indenter, the back-shear flattens to horizontal (Fig. 7a, b and d), whereas models with moderate local deposition provide support so that their back-shears maintained a dip near 30° (Fig. 7c). As the rigid indenter has the angle of internal friction of the sand, no effective indenter developed in any of these models (cf. Bonini et al., 1999; Persson, 2001). The face of the rigid indenter acted as the active plane of shear throughout the deformation.

5.6. Models with rigid indenter face dips of 15°

By 10% bulk shortening, all models had developed a back-shear slightly above the rigid indenter ($\beta \approx 20°$) and two fore-kinks (Fig. 8). Three fore-kinks and one back-shear had developed by 20% bulk shortening (Fig. 8). By 40% bulk shortening, only the model with total erosion differed from the others having developed seven fore-kinks instead of six (Fig. 8). All eroded models developed smaller effective indenters than models without erosion. The front face of the effective indenter where no erosion was applied had a dip of 28°, whereas the other models developed a back-shear dipping about 20° (Fig. 8). The fore-kinks initiated with dips in the range of 28–32°.

5.7. Models with asymmetric erosion

In models with asymmetric erosion, the erosion was concentrated on the back-wedge (Fig. 9a). Only models with a rigid indenter face dip of 75° are

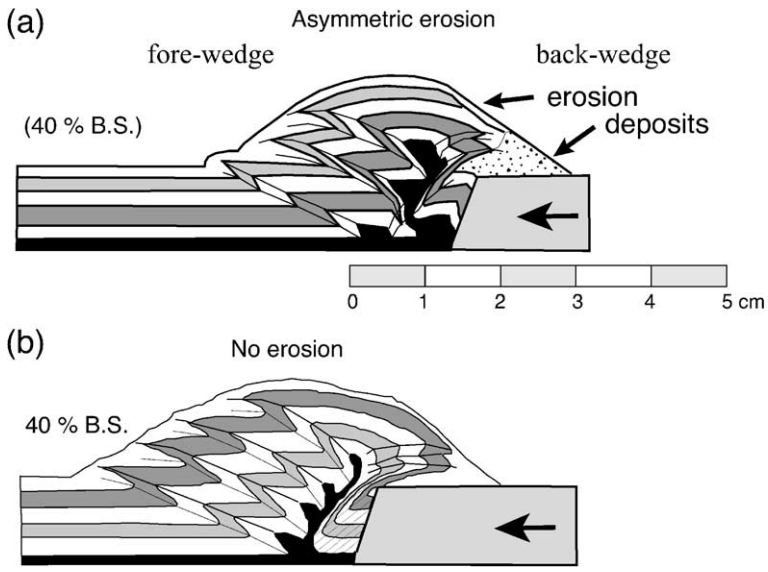

Fig. 9. Sketch of models where a rigid indenter face dips at 75° after 40% bulk shortening (a) asymmetric erosion of the back-wedge and local deposition above the rigid indenter, and (b) no erosion.

presented here. In these models, the initiation of new fore-kinks was delayed compared to models without erosion (cf. Fig. 9a and b). Only three fore-kinks had developed by 40% bulk shortening, where the first two clearly had steepened and back-rotated as they had been carried up the only back-shear. An effective indenter developed behind a back-shear with a dip of about 50°. Erosion on the back-wedge unloaded the back-shear, which consequently stayed active for longer. This also affected the fore-kinks, which were longer-lived and back-rotated further than in models without erosion.

6. Discussion

Erosion and redeposition changes the pattern of strain partitioning in and around the model orogenic wedge and therefore affects both the thrust geometry and the vertical extrusion rate. Redistributing the load from the top of the wedge to its margins disturbs wedge development.

Models with rigid indenter dips of 75° produce fewer fore-kinks that remain active for longer if erosion is applied. The local decrease in load disturbs the development of the critical taper. The wedge undergoes forward and vertical compaction and shear until it reaches a critical taper that locks movement along the shear. Decreasing the load on the active shear plane allows it to shear further before it locks (cf. also Cobbold et al., 1993; Merle and Abidi, 1995). Local redeposition of the eroded material increases the vertical load further from the wedge and contributes to the higher efficiency of strain partitioning along the existing shear plane instead of developing a new shear. However, not all models produce fewer kinks as a result of erosion. Models with rigid indenter dips of 15° and total erosion develop only one more kink by 40% bulk shortening than models without erosion. These models develop a very small effective indenter, and the volume of sand to laterally compact is smaller so that strain partitions by imbricate shear rather than compaction. Additionally, no effective indenter develops in models with rigid indenter dips of 75° and moderate erosion with local deposition, nor in those in which the extruding portion of the rising wedge was removed as fast as it rose. The growth of effective indenters therefore depends not only on the face dip of the rigid indenter (Bonini et al., 1999; Persson, 2001), but also on the amount of erosion. Only in model convergence zones with limited or no erosion are effective indenters well developed. For models with rigid indenter dips of 30° and total erosion, there was no redeposition to increase the vertical loads on the foreland and hinterland. This lack of redeposition eased the formation of new kinks and, consequently, more kinks developed than in models with sedimentation. Strain partitioning is clearly a close interplay between the mechanism of compaction, slip along a décollement and slip along imbricate shears/kinks, all of these depending on the rate of erosion and amount of redeposition in the vicinity of the wedge.

If models resemble nature and the vertical front face of the stiffer continent falls above 30°, the more the erosion, the longer decreasing numbers of successive shears remain active. As a consequence, areas with rapid erosion will enable high ratios of vertical vs. lateral (orogen normal) escape of the orogenic wedge. The extreme case, of total erosion and removal, is unlikely in nature. This case produces no mountains to localize rainfall and enhance erosion, and no slopes are generated to localize gravity-controlled denudation or mechanical erosion. However, the model with total erosion and rigid indenter dip of 75° produces efficient upward escape of deep crust towards shallow levels.

The models described here suggest that erosion above an active shear favors continued movement on the same shear, aiding upward transport of deep material. Equivalent transport of crustal material of high-grade rocks is seen in the Southern Alps of New Zealand (Koons, 1990). The Southern Alps, a narrow mountain range with summits' heights up to 3470 m, has formed within the last 5 Ma. The Australian plate acts as a rigid indenter converging with the Pacific plate, which is translated southwestward parallel to the Alpine Fault (Fig. 10) and is obliquely thrust up and over the Australian plate (Norris et al., 1990; Koons, 1990). Immense erosion on the northwestern side (Fig. 10) of the orogen induced by heavy rainfall (Griffiths and McSaveney, 1983; Norris and Cooper, 1997) has exhumed high-grade hanging wall schist and gneisses at rates of 5–10 mm/year (Norris and Cooper, 1997 and references therein). Schists of amphibolite faces have been exhumed from depths of 20–25 km during the last 2–3 Ma; they now crop

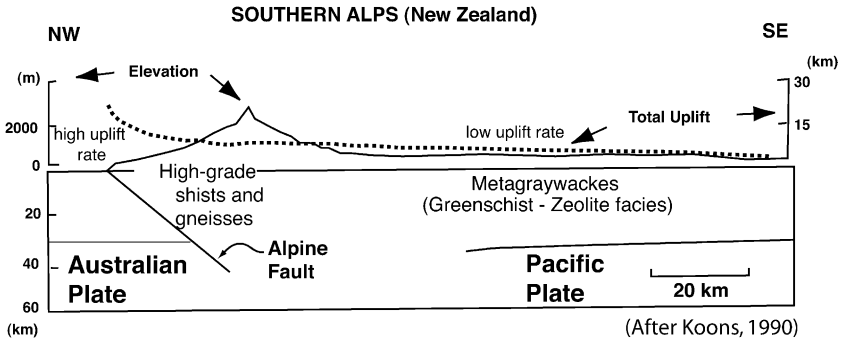

Fig. 10. Schematic profile of the Southern Alps, New Zealand (from Koons, 1990). Immense erosion on the northwestern side of the orogen has been linked to high transport rates along the Alpine Fault where now high-grade hangingwall schist and gneisses are exposed.

out as a narrow strip along the western side of the Southern Alps, beside the Alpine Fault (Norris and Cooper, 1997; Koons 1990) (Fig. 10). A thrust segment of the Alpine Fault, the Waikukupa thrust, has emplaced mylonites and cataclasites over fluvial–glacial gravel (Norris and Cooper, 1997). The average slip-rate of the Hare Mare Thrust on the eastern side of the Waikukupa river valley and the Waikukupa thrust is estimated at 22–30 mm/year (Norris and Cooper, 1997).

Like in the Southern Alps, rates of erosion are not likely to be as symmetrical over real mountain belts as the erosion applied in most of the sandbox models. The Southern Alps (New Zealand), Himalaya and Western European Alps are all subject to rapid erosion on the side of the rising orogenic wedge facing the indenter, i.e., on the back-wedge (Fig. 1). In these areas, the greatest erosion is close to the indenter, where the rainfall is heaviest and the streams are most concentrated. The highest uplift rate is therefore close to the indenter and not where the mountains are highest (Koons, 1990). However, asymmetry in uplift is caused not only by variations in erosion rates, it is also a result of the asymmetric pattern of fore- and back-shears inside the wedge. Strain is focussed along a single long-lived and constantly reactivated back-shear, on one side, and divided among a succession of comparatively short-lived fore-kinks, on the other. Furthermore, the rapid rise of deep, hot material in the back-wedge supplies thermal energy close to the indenter. This leads to an orogen in which mechanical and thermal energies are strongly partitioned into the high-strain regions of the back-wedge (Koons, 1987, 1990). Our models further emphasize the importance of where the erosion takes place. Erosion remote from an active thrust is not likely to influence the length of activity along it. However, erosional unloading of the hanging wall above an active thrust allows that particular thrust to stay active for longer.

7. Conclusions

Tectonic plate movements resulting in topographic highs and lows have long been known to control the circulation of the atmosphere and ocean and therefore influence the climate. However, climate also controls rates of erosion and therefore tectonics. As shown here, erosion influences the slip-rate and active lifetimes of faults and therefore controls the development of thrust patterns within orogenic wedges. Of great importance is where the erosion and deposition take place. Thrusts unloaded by erosion will remain active for longer and is clear for models with rigid indenter dips of $\geq 45°$. Redeposition of eroded material can further expand the lifetime of the already active thrust as the load hinders initiation of new shears beneath the additional depositional load. However, models with low-angle rigid indenter dips initiate equal or greater amount of thrust if erosion is applied. This, as erosion, favors thrusting rather than compaction and decreases the size and relevance of effective indenters. The tectonic effect of erosion is therefore also controlled by the shape of the rigid indenter. Models here suggest that there may come a time when profiles across orogenic wedges can be used to discuss past climates.

Acknowledgements

Gracious thanks to Prof. Jean-Pierre Burg, Associate Prof. Genene Mulugeta, Prof. Christopher Talbot, Prof. P.R. Cobbold and Dr. J. Vergés for their comments on both Science and English. K. Persson greatly appreciates the financial support of a "doktorandtjänst" from Uppsala University. D. Sokoutis kindly acknowledges the financial support from The Netherlands Centre for Integrated Solid Earth Science (ISES) and The Netherlands Organization for Scientific Research (NWO).

References

Beaumont, C., Fullsack, P., Hamilton, J., 1992. Erosional control of active compressional orogens. In: McClay, K.R. (Ed.), Thrust Tectonics. Chapman & Hall, London, pp. 1–18.

Bonini, M., Sokoutis, D., Talbot, C.J., Boccaletti, M., Milnes, A.G., 1999. Indenter growth in analogue models of Alpine-type deformation. Tectonics 18, 119–128.

Byerlee, J., 1978. Friction of rocks. Pure and Applied Geophysics 116, 615–626.

Cobbold, P.R., Davy, P., Gapais, D., Rossello, E.A., Sadybakasov, E., Thomas, J.C., Tondji Bijo, J.J., de Urreiztieta, M., 1993. Sedimentary basins and crustal thickening. Sedimentary Geology 86, 77–89.

Colletta, B., Letouzey, J., Pinedo, R., Ballard, J.F., Balé, P., 1991. Computerized X-ray tomography analysis of sandbox models: examples of thin-skinned thrust systems. Geology 19, 1063–1067.

Dahlen, F.A., 1988. Mechanical energy budget of a fold- and-thrust belt. Nature 331 (6154), 335–337.

Davis, D., Suppe, J., Dahlen, F.A., 1983. Mechanics of fold- and-thrust belts and accretionary wedges. Journal of Geophysical Research 88, 1153–1172.

Davy, C., Cobbold, P.R., 1988. Indentation tectonics in nature and experiment: 1. Experiments scaled for gravity. Bulletin of the Geological Institutions of the University of Uppsala 14, 129–141.

Davy, C., Cobbold, P.R., 1991. Experiments on shortening of a 4-layer model of the continental lithosphere. Tectonophysics 188, 1–25.

Goodman, R.E., 1988. Introduction to Rock Mechanics. Wiley, Chichester. 576 pp.

Griffiths, G.A., McSaveney, M.J., 1983. Distribution of mean annual precipitation across some steepland regions of New Zealand. New Zealand Journal of Science 26, 197–209.

Huiqi, L., McClay, K.R., Powell, D., 1992. Physical models of thrust wedges. In: McClay, K.R. (Ed.), Thrust Tectonics. Chapman & Hall, London, pp. 71–81.

Koons, P.O., 1987. Thermal and mechanical consequences of rapid uplift in continental collision: an example from Southern Alps. Earth and Planetary Science Letters 86, 307–319.

Koons, P.O., 1990. Two-sided orogen: collision and erosion from sandbox to the Southern Alps, New Zealand. Geology 18, 679–682.

Koyi, H., 1995. Mode of internal deformation in sand wedges. Journal of Structural Geology 17, 293–300.

Krantz, R.W., 1991. Measurements of friction coefficients and cohesion for faulting and fault reactivation in laboratory models using sand and sand mixtures. Tectonophysics 118, 203–207.

Kusznir, N.J., Park, R.G., 1984a. Intraplate lithosphere deformation and the strength of the lithosphere. Geophysical Journal of the Royal Astronomical Society 79, 513–538.

Kusznir, N.J., Park, R.G., 1984b. The strength of intraplate lithosphere. Physics of the Earth and Planetary Interiors 36, 224–235.

Malavieille, J., 1984. Modélisation expérimentale des chevauchements imbriqués: application aux chaînes de montagnes. Bulletin de la Société Géologique de France 7, 129–138.

Mandle, G., 1988. Mechanics of Tectonic Faulting: Models and Basics Concepts Elsevier, Amsterdam. 407 pp.

Marshak, S., Wilkerson, M.S., 1992. Effect of overburden thickness on thrust belt geometry and development. Tectonics 11, 560–566.

Merle, O., 1994. Syn-convergence exhumation of the central Alps. Geodinamica Acta 7 (3), 129–138.

Merle, O., Abidi, N., 1995. Approche expérimentale du fonctionnement des rampes émergentes. Bulletin de la Société Géologique de France 166, 439–450.

Mulugeta, G., 1988. Modelling the geometry of Coulomb thrust wedges. Journal of Structural Geology 10, 847–859.

Mulugeta, G., Koyi, H., 1987. Three-dimensional geometry and kinematics of experimental piggyback thrusting. Geology 15, 1052–1056.

Mulugeta, G., Koyi, H., 1992. Episodic accretion and strain partitioning in a model sand wedge. Tectonophysics 202, 319–333.

Norris, R.J., Cooper, A.F., 1997. Erosional control on the structural evolution of a transpressional thrust complex on the Alpine Fault, New Zealand. Journal of Structural Geology 19, 1323–1342.

Norris, R.J., Koons, P.O., Cooper, A.F., 1990. The obliquely-convergent plate boundary in the South Island of New Zealand: implications for ancient collision zones. Journal of Structural Geology 12, 715–725.

Persson, K.S., 2001. Effective indenters and the development of double-vergent orogens: insights from analogue sand models. In: Koyi, H.A., Mancktelow, N.S. (Eds.), Tectonic Modeling: A Volume in Honor of Hans Ramberg. Boulder, Colorado. Memoir - Geological Society of America Memoir, vol. 193, pp. 191–206.

Ratschbacher, L., Merle, O., Davy, P., Cobbold, P., 1991. Lateral extrusion in the eastern Alps: Part 1. Boundary conditions and experiments scaled for gravity. Tectonics 10, 245–256.

Sonder, L.J., England, P., 1986. Vertical averages of rheology of the continental lithosphere: relation to thin sheet parameters. Earth and Planetary Science Letters 77, 81–90.

Storti, S., Salvini, F., McClay, K., 2000. Synchronous and velocity-partitioned thrusting and thrust polarity reversal in experimen-

tally produced, doubly-vergent thrust wedges: implications for natural orogens. Tectonics 19, 378–396.

Tapponnier, P., Molnar, P., 1976. Slip-line field theory and large-scale continental tectonics. Nature 264, 319–324.

Tapponnier, P., Pelzer, G., Le Dain, A.Y., Armijo, R., Cobbold, P., 1982. Propagating extrusion tectonics in Asia: new insights from simple experiments with plasticine. Geology 10, 611–616.

Thompson, A.B., Schulmann, K., Jezek, J., 1997. Extrusion tectonics and elevation of lower crustal metamorphic rocks in convergent orogens. Geology 6, 491–494.

Weijermars, R., Schmeling, H., 1986. Scaling of Newtonian and non Newtonian fluid dynamics without inertia for quantitative modeling of rock flow due to gravity (including the concept of rheological similarity). Physics of the Earth and Planetary Interiors 43, 316–330.

Willett, S., Beaumont, C., Fullsack, P., 1993. Mechanical model for the tectonics of doubly vergent compressional orogens. Geology 21, 371–374.